Biosensors and Bioelectronics 194 (2021) 113625

Contents lists available at ScienceDirect

Biosensors and Bioelectronics

journal homepage: www.elsevier.com/locate/bios

DNAzyme based three-way junction assay for antibody-free detection of locus-specific N^6-methyladenosine modifications

Hongyan Yu [a,1], Qinli Pu [a,b,1], Zhi Weng [a,1], Xi Zhou [a], Junjie Li [a], Yujun Yang [a], Wang Luo [a], Yongcan Guo [c], Huajian Chen [a,d], Ding Wang [a,e], Guoming Xie [a,*]

[a] Key Laboratory of Clinical Laboratory Diagnostics (Chinese Ministry of Education), College of Laboratory Medicine, Chongqing Medical Laboratory Microfluidics and SPRi Engineering Research Center, Chongqing Medical University, No. 1 Yi Xue Yuan Road, Chongqing, 400016, PR China
[b] Department of Laboratory Medicine, The Second Affiliated Hospital of Chongqing Medical University, Chongqing, 400010, PR China
[c] Department of Laboratory Medicine, Affiliated Traditional Chinese Medicine Hospital of Southwest Medical University, Luzhou, 646000, China
[d] Chongqing Emergency Medical Center, Chongqing University Central Hospital, School of Medicine, Chongqing University, Chongqing, China
[e] Shanghai Upper Bio Tech Pharma Co.,Ltd., Shanghai, 201201, China

ARTICLE INFO

Keywords:
Isothermal nucleic acid amplification
Electrochemical sensor
CRISPR-Cas12a
DNAzyme
N^6-methyladenosine

ABSTRACT

N^6-methyladenosine (m6A) is the most abundant post-transcriptional modification in RNA and has important implications in physiological processes and tumor development. However, sensitive and specific quantification of locus-specific m6A modification levels remains a challenging task. In the present work, a novel m6A-sensitive DNAzyme was utilized to directly detect m6A by coupling with a three-way junction-mediated isothermal exponential CRISPR amplification reaction for the first time. This method was built on the fact that the binding arm of the DNAzyme bound to the specific site and its core structure catalyzed the selective cleavage of unmodified adenine instead of methylated adenines. Subsequently, the intact RNA was identified by the proximity effect of the three-way junction. Enormous amounts of single-stranded DNA products were generated through a combination of SDA and EXPAR for signal amplification. The specific real-time curve of products was recorded through detecting the fluorescence intensity triggered by CRISPR Cas12a. As a result, methylation target of abundance down to 1% was successfully identified. In addition, this strategy could be used for the analysis of cell RNA extracts. Combined with an electrochemical sensor for quantitative detection of RNA methylation, we demonstrated the generality of as-proposed strategy. We envision the present method would provide a new platform for the analysis of m6A in RNA and promote its application in clinical diseases.

1. Introduction

More than 170 types of RNA chemical modifications have been collected in MODOMICS database (Boccaletto et al., 2018). As the most abundant forms of post-transcriptional RNA modification, N^6-methyladenosine (m6A) was found in messenger RNA (mRNA) (Deng et al., 2015), ribosomal RNA (rRNA) (Choi and Busch, 1978) and long non-coding RNA (lncRNA) (Alarcón et al., 2015) of eukaryotes and bacteria. The dynamic and reversible regulation of m6A modification between methyltransferase and demethylases has made the research of RNA epigenetics arouse great interest (Jia et al., 2011; Wang et al., 2016a). It suggests that m6A modifications have profound implications for gene expression, including pre-mRNA splicing, pri-miRNA processing, mRNA translation and degradation (Liu et al., 2019). Some studies have shown that specific locus dysregulation of m6A modifications was associated with bacterial infection and the progression of cancer (Deng et al., 2018). Thus, a simple and efficient method to accurately detect the m6A modification is of great significance to elucidate the mechanisms of m6A regulation in related diseases.

Unlike bases such as m7G and m1A (Ding et al., 2020; Marchand et al., 2018), m6A is only methylated on its exocyclic amino groups, which makes m6A similar to adenosine in chemical properties. Methylation information is lost during reverse transcription and there is still a lack of chemical methods like bisulfite treatment of m5C to distinguish m6A from A (Squires et al., 2012). Moreover, m6A in clinical specimens is usually of low abundance (Wei et al., 1975). To surmount

* Corresponding author. .
E-mail addresses: guomingxie@cqmu.edu.cn, xiegm059@foxmail.com (G. Xie).
[1] Hongyan Yu, Qinli Pu and Zhi Weng contributed equally to this work.

https://doi.org/10.1016/j.bios.2021.113625
Received 6 June 2021; Received in revised form 6 September 2021; Accepted 10 September 2021
Available online 11 September 2021
0956-5663/© 2021 Elsevier B.V. All rights reserved.

the challenges mentioned above, liquid chromatography coupled to tandem MS (LC-MS/MS) and high-throughput sequencing have been proposed to detect m6A modification. Although global m6A levels are assessed, LC-MS/MS does not provide the localization information of the m6A modification (Fu et al., 2015; Huang et al., 2016). To map the transcriptome of mRNA modifications, researchers have developed m6A-RNA immunoprecipitation sequencing (MeRIP-seq or m6A-seq), PA-m6A-seq, miCLIP and m6A-CLIP (Dominissini et al., 2012; Meyer et al., 2012; Chen et al., 2015; Linder et al., 2015). These transcriptome-wide techniques rely on m6A-specific antibodies, suffering from cross-reactivity of m6A antibodies with m6Am. In addition, quantitative information on modification levels could hardly be revealed. The ability to quantify m6A modifications at single-base resolution is essential for revealing new insights between m6A and human diseases. RNase H cleavage-based strategy named SCARLET (site-specific cleavage and radiolabeling followed by ligation-assisted extraction and thin-layer chromatography) is the earliest method to quantitatively detect the m6A status at a specific site (Liu et al., 2013). However, radiolabeling and complicated procedures hinder its application in rapid m6A detection. Additionally, based on reverse transcription in the presence of polymerase (TthDNA polymerase or BstDNA polymerase) or SeTTP (Harcourt et al., 2013; Hong et al., 2018; Wang et al., 2016b), some methods have been proposed to prefer extension of unmodified sites. Generally, the approach involves characterizing m6A by electrophoresis, lacking an amplification procedure. Therefore, a convenient and reliable method to quantify the degree of m6A with single-base resolution is still in urgent need.

Specific discrimination of m6A from its unmethylated counterpart is essential for high-performance m6A analysis. As an attractive alternative to enzymes and antibodies, a group of m6A-sensitive DNAzyme was identified by Claudia Höbartner's group via *in vitro* selection, which both have site-specificity and endonuclease activity (Sednev et al., 2018). It can specifically recognize and cleave A-containing RNA with reasonably robust efficiency, but not m6A-containing RNA. Otherwise, the cleavage function of the DNAzyme (VMC10) allows the regulation of three-way junction (TWJ) formation for biosensing purposes. The simple and elegant identification way supplies a novel perspective for detecting RNA modification.

As target m6A modification is frequently accompanied with abundant concomitant interfering nucleosides, it is necessary to apply signal amplification strategies to selectively enhance signal output upon target m6A recognition. The clustered regularly interspaced short palindromic repeats (CRISPR)/Cas immune system is a promising platform for nucleic acid detection because of its high specificity and efficiency (Dai et al., 2019; Makarova et al., 2011; Yuan et al., 2020; Zetsche et al., 2015). In our previous work, CRISPR Cas12a-based gene editing systems has been successfully constructed for non-DNA targets in ultralow concentrations (Li et al., 2020). In addition, by combining nucleic acid amplification with CRISPR Cas12a, nucleic acid detection with higher sensitivity would be achieved (Peng et al., 2020; Xing et al., 2020). Exponential amplification reaction (EXPAR), as a representative isothermal reaction, is widely used by the reason of high amplification efficiency (10^8-fold) and fairly simple procedure (Jia et al., 2010). Thus, the integrated EXPAR−Cas12a system not only improves the sensitivity but also provides the opportunity to monitor the products in a real-time manner.

Herein, we reported an antibody-free approach for precise detection of m6A in locus-specific RNA by combining a novel m6A-sensitive DNAzyme with a three-way junction-induced exponential CRISPR reaction (TWJ-ECR). The methylation-sensitive DNAzyme was used to identify and cleave the unmethylated RNA, while TWJ structures could only be formed in the presence of the retained intact methylated RNA. Subsequently, released DNA fragment from strand displacement amplification (SDA) triggered EXPAR which afford a high quadratic amplified signal. Then, the products were detected by CRISPR reaction system, enabling us to further amplify the signal and monitor the reaction specifically. Regarding the need for detection in resource-limited settings, the strategy was applied to electrochemical sensors successfully. Furthermore, we performed the assay in serum to validate the practical application of the method in complex biological samples. To the best of our knowledge, this is the first report of isothermal amplification-based real-time m6A RNA detection. We envision that this method would provide a new insight for site-specific m6A RNA quantification and be further applied to laboratory and clinical RNA methylation research.

2. Experimental

The reagents, instruments, and specific experimental steps were listed in supplementary material.

3. Results and discussion

3.1. Principle of the DNAzyme based TWJ-ECR method for the detection of m6A RNA

Fig. 1 schematically illustrated the working principle of the DNAzyme based TWJ-ECR approach to detect RNA m6A modifications in a given locus. It utilized the high specificity of DNAzyme (VMC10) to cleave unmethylated adenine sites and the high sensitivity of TWJ-ECR for efficient amplification of the cleavage products. m6A at the 2577th site of MALAT1(metastasis associated lung adenocarcinoma transcript 1) lncRNA, which has been identified to contain an m6A modification (Liu et al., 2013), was employed as the model site-specific methylated RNA target in this study. As shown in Fig. 1, for detection of m6A modifications, two simple steps were involved in the DNAzyme-based cleavage of RNA and sequential TWJ-ECR amplification. The methylated RNA (RNA2577-m6A) and the unmethylated RNA (RNA2577-A) were incubated with the DNAzyme. The unmethylated RNA site GGACU would be recognized and cleaved in the middle of the sequence GG-ACU by DNAzyme, while the methylated RNA site GGm6ACU remains intact.

In the presence of intact target RNA2577-m6A, the short domain II (crimson) of TWJ probes formed a stable double-strand structure in proximity by displacing the recognition arm of DNAzyme from intact RNA through toehold exchange reaction. With the assistance of Bst DNA Polymerase (BST) and deoxyribonucleoside triphosphates (dNTPs), the TWJ primer would extend along with the TWJ template containing the recognition site of the nicking endonuclease Nt.BsrDI. Thus, the extension, nicking and strand displacement would repeat continuously through the 3' -end of TWJ-primer, releasing vast short oligonucleotides (X strands) as "trigger" (cycle 1).

EXPAR was initiated when the "trigger" hybridized with its complementary sequence at the 3′-terminus of the EXPAR template and then extended along the template under the catalysis of Bst DNA polymerase. Meanwhile, two recognition sequences for Nt.BsrDI were generated. The same restriction enzyme was used for improving reaction efficiency. Subsequently, the nicking enzyme recognized the site, cleaved the DNA duplex and released a short oligonucleotide with the same X strands and Y strands repeatedly. In the meantime, the released X oligonucleotide can hybridize with other EXPAR templates to perform new cycles of extension, cleavage, and strand displacement reactions, producing massive Y strands (cycle 2 and 3). These reactions turn the linear reaction into exponential amplification mechanism. Finally, the real-time fluorescence curves were monitored through trans-cleavage activity of CRISPR activated by Y strands.

In contrast, when a cleaved target RNA2577-A was present, the TWJ-probes could not form a stable structure as the melting temperature of the shorter complementary sequence in domains II was set well below the reaction temperature. Besides, because DNAzyme cleaved the RNA phosphodiester bond to produce a forward fragment with 2′ and 3′ cyclic phosphate groups, the extension of RNA at the 3′-end would be blocked.

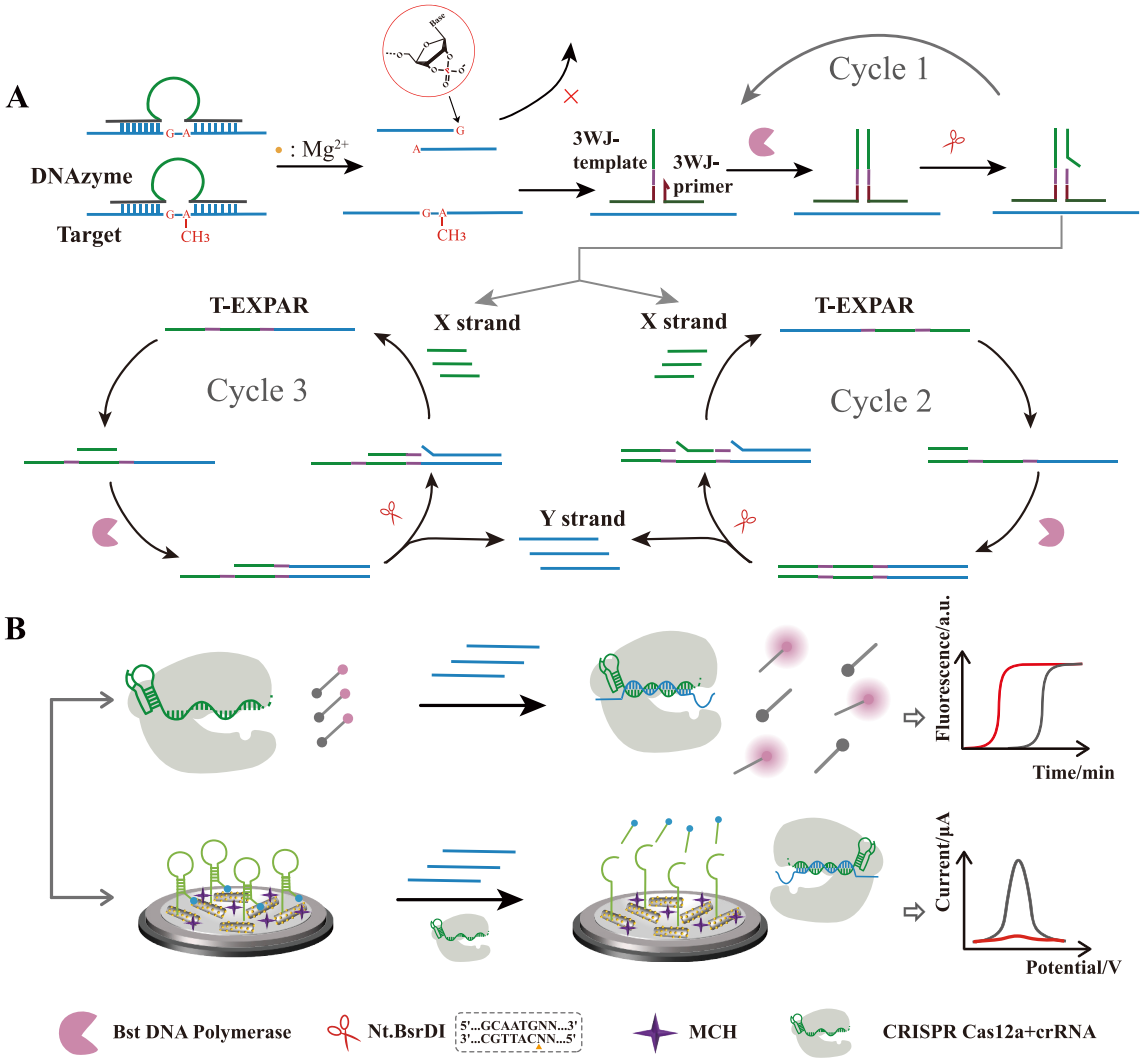


Fig. 1. Schematic illustration of a novel DNAzyme and three-way junction-induced exponential CRISPR reaction for the detection of locus-specific N6-methyladenosine modifications.

3.2. Design and characterization of three-way junction assay

In order to detect the intact methylated RNA, two TWJ DNA probes comprised of TWJ primer and TWJ template were rationally designed where the sequence comprised of four domains, respectively. The domain I in TWJ-probes was designed to be complementary to a part of the target RNA (dark green). The domain II (crimson) of TWJ-probes only possessed 7-bp long complementary sequences. There were two "T" bases in the TWJ primer that formed an additional nucleotide bulge loop at the junction, which enhanced the thermodynamic stability of TWJ (Kong et al., 2011). The domain III (purple) contained a nicking enzyme Nt.BstNBI recognition site. The domain Ⅳ (fresh green) in TWJ-template served as "track" for elongation. Besides, the 3′-end of TWJ-template was modified with phosphate group to inhibit non-specific amplification (Murakami et al., 2012). The T-EXPAR template was designed as X'N'X'N'Y'. Y′ was complementary to the sequence of crRNA and N′ contained a complementary site for Nt.BsrDI nicking.

Firstly, we verified the formation of the three-way junction by NuPack for simulation (Fig. S1A) and melting curve analysis using SYBR Green I (Fig. S1B). When target RNA and TWJ probes were mixed, strong fluorescent intensity was observed at 64.6 °C, demonstrating that the stable TWJ structure was formed at the reaction temperature of TWJ-ECR (46 °C). Similar melting curves were measured between RNA and either of TWJ probes. The observed melting temperatures were 56.6 °C for TWJ primer and 64.4 °C for TWJ template. In contrast, when only TWJ probes were mixed, much weaker fluorescent intensity was obtained, suggesting that no double strand was formed without RNA.

The results were further confirmed by a non-denaturing polyacrylamide gel (PAGE) data in Fig. S1C. The TWJ structure was only seen in lane 1, containing both the TWJ probes and the target RNA. There was no sign of binding between the three-way junction template and primer in line 4 without RNA. The complexes of target hybridized with TWJ template or primer were correctly observed in lanes 2 and 3, respectively. All the results of PAGE proved that the TWJ structure was formed only in the presence of all three components.

3.3. Feasibility of DNAzyme and TWJ-induced exponential amplification reaction

According to our design principle, the ability of DNAzyme for highly specific methylation recognition was essential for the proposed DNAzyme based TWJ-ECR analysis. The sequence of DNAzyme (VMC10) was shown in Fig. 2A. It contained an RNA-cleaving catalytic core flanked by two RNA-recognition binding arms (11 nt on the left and 10 nt on the right). The design of the core sequence endowed the DNAzyme with preference for cleaving the unmethylated RNA instead of methylated RNA. The length of the binding arms on both sides was designed to bind

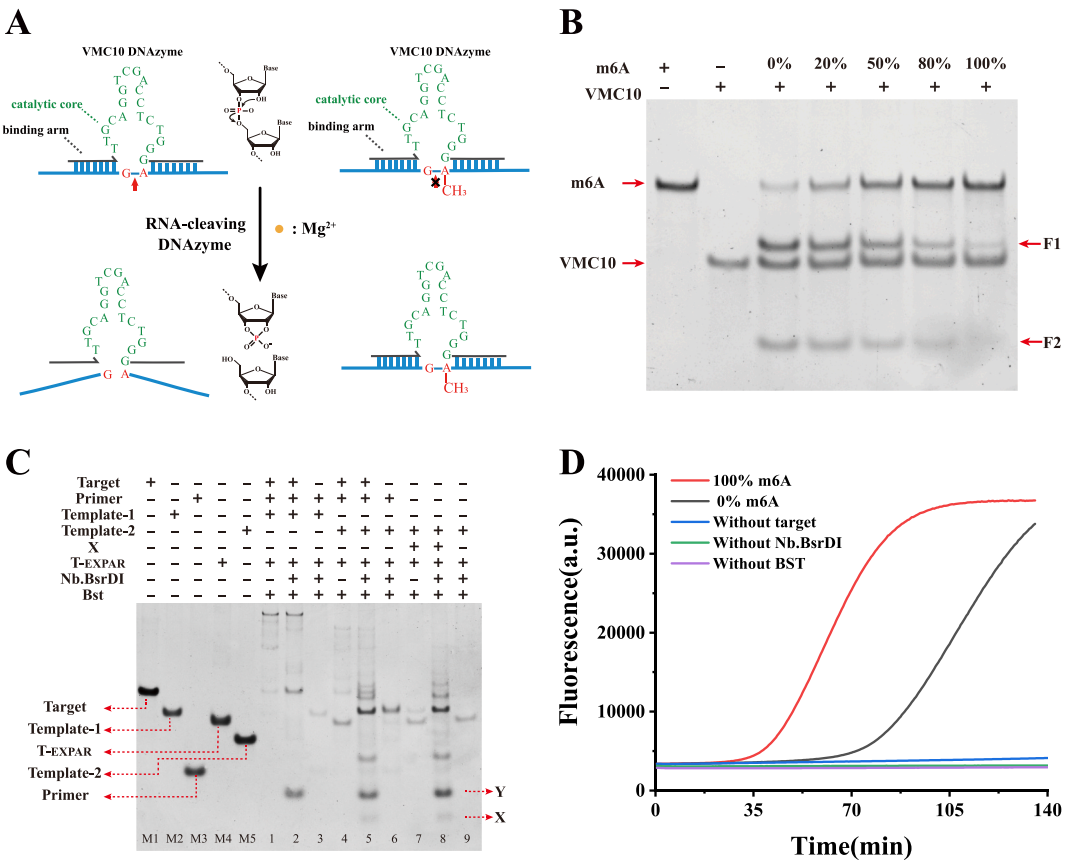


Fig. 2. DNA-catalyzed cleavage of MALAT1-2577RNA. (A) RNA-cleaving DNAzyme (VMC10) sequences and RNA cleavage reaction. The red arrows indicate the cleavage site. (B) PAGE analysis of cleavage products containing varied m6A fraction. Feasibility of TWJ-ECR reaction. (C) PAGE image of the products obtained after 50 min (line 1,2,3) for SDA, 20 min (line 4,5,6,7,8,9) for EXPAR and TWJ-ECR reaction, respectively. (The '+' and '-' denote the presence and absence of the corresponding components, respectively). (D) Real-time fluorescence monitoring of TWJ-ECR reaction with CRISPR Cas12a as the fluorescent indicator. (For interpretation of the references to colour in this figure legend, the reader is referred to the Web version of this article.)

RNA without falling off, and be replaced by the TWJ probes. We verified the feasibility of DNAzyme cleavage and the cleavage efficiency on RNA with various modified degrees. The results were analyzed by PAGE in Fig. 2B. As the degree of methylation continued increasing, the cleavage products continued decreasing, indicating that m6A-sensitive DNAzyme identified the locus-specific m6A modifications specifically.

Subsequently, to verify the feasibility of the constructed amplification strategy, PAGE was employed to analyze the resultant products of TWJ-structure triggered SDA (lane 1–3), the isothermal exponential amplification reaction (EXPAR) (lane 7–9), and three-way junction-induced exponential amplification reaction (lane 4–6), respectively. As illustrated in Fig. 2C, the products (Y strand) of SDA were generated only in the presence of a target (line 2). The lack of a target (line 3) or Nt.BsrDI (line 1) cannot trigger the reaction to proceed, as well as EXPAR in the presence of trigger (X strand) (line 8), and in the absence of trigger (line 9) or Nt.BsrDI (line 7). The feasibility of combining SDA with EXPAR was confirmed. The Y strands and X strands were clearly seen in band 5 (with target), whereas no product was observed in band 6 (without target) and band 4 (without Nt.BsrDI). These results demonstrated that the trigger had smoothly generated in the process of SDA reaction and activated EXPAR to generate Y stands.

3.3.1. Fluorescence detection of TWJ-ECR

In order to further amplify the signal and detect m6A modifications in a real-time, we monitored the fluorescence by adding CRISPR Cas12a into the reaction system. Compared with SYBR Green (Jiang et al., 2015), CRISPR Cas12a only generates a fluorescent signal when triggered by specific sequence. To explore whether the TWJ-ECR was properly operated as we designed, we conducted the TWJ-ECR in the presence of the positive group with methylated RNA, the negative group with unmethylated RNA, the blank group without any targets and the control group without Bst DNA Polymerase or Nt.BsrDI nicking endonuclease. The real-time fluorescence signals generated by trans-cleavage activity of CRISPR Cas12a were measured. As is shown in Fig. 2D, the control group shown almost no gain of fluorescence, furnishing proof of the essential roles played by Bst DNA Polymerase and Nt.BsrDI nicking endonuclease in the sensing system. The blank group provided similar weak fluorescence signals. It was noticed that nearly no background was seen by this sensing platform. On the contrary, in the presence of RNA2577-m6A, the fluorescence intensity reached the equilibrium much faster than that with the unmethylated counterpart. This confirmed that the amplification efficiency of methylated RNA was significantly higher than unmethylated RNA. The threshold time difference (ΔTt) of amplification was over 46. On the basis of these results, it was reasonably concluded that the selected DNAzyme had superior performance in recognizing methylation and TWJ-ECR method was feasible for the accurate and highly specific detection of site-specific m6A modifications.

As depicted in Fig. 3A, although generation of X strands was inherently linear, the subsequent X-triggered EXPAR reaction generated lots of Y strands through the exponential amplification mechanism. To demonstrate the amplification efficiency of TWJ-ECR, a control experiment of SDA process was carried out. It can be seen that target-triggered fluorescence signal of TWJ-ECR was much higher than that of SDA process. A high signal enhancement of 7.7-fold was observed in TWJ-ECR, whereas only a 1.4-fold signal increase was achieved by the SDA

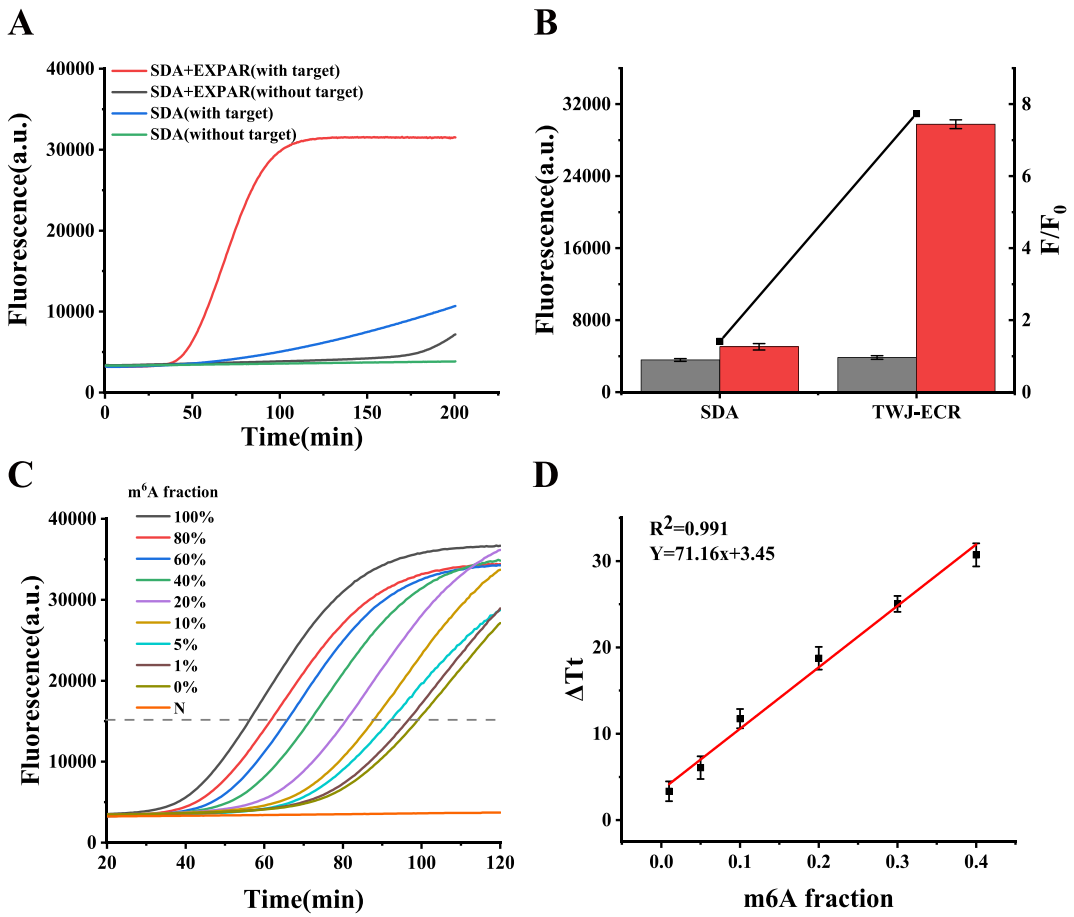


Fig. 3. Confirmation of the amplification efficiency of TWJ-ECR. (A) Real-time fluorescence curves and (B) the fluorescence responses of basic SDA and TWJ-ECR. Analytical performance of the optimized DNAzyme based TWJ-ECR for determining m6A fraction. (C) Real-time fluorescence amplification curves with different ratios of m6A. (D) The linear relationship between the ΔTt values and the m6A fraction from 1% to 40%. Error bars were estimated from triplicated independent experiments.

(Fig. 3B). The above results illustrated that TWJ-ECR could provide a higher signal by exponential amplification reaction than basic SDA.

3.3.2. Fluorescence analytical performance of the TWJ-ECR method for m6A RNA detection

Although the cleavage of DNAzyme was impossible without background leakage, the concentration of the enzyme could be carefully optimized to maximize the difference between unmethylated and methylated RNA (Fig. S2). As a compromise of specificity and reaction efficiency, 0.01 U/μL polymerase and 0.2 U/μL nicking endonuclease was selected for subsequent TWJ-ECR assay. The reaction buffers and temperature were also optimized in Fig. S3. The optimal conditions were in CutSmart buffer at 46 °C.

Under optimized conditions, the performance of the proposed TWJ-ECR strategy for quantitative evaluation of various m6A methylation levels was assessed in a real-time manner. Firstly, RNA2577-A and RNA2577-m6A were mixed in specific proportions in the range from 0% to 100% with a constant total DNA concentration in simulated samples. Similar to the threshold cycle (Ct) in real-time fluorescent quantitative PCR, we defined the time when the fluorescence intensity exceeded the set threshold line as the threshold time (Tt). Fig. 3C revealed that as the ratio of RNA2577-m6A increased, the fluorescence curve arose rapidly, indicating the detected TWJ-ECR product depended on the initial degree of the m6A modifications. Furthermore, this DNAzyme based TWJ-ECR assay could detect 1% methylation level in the presence of a large excess of unmethylated RNA. The features provided by the developed TWJ-ECR assay are compared with those of the strategies reported so far for the determination of m6A (Table S2). It is much lower than most of the conventional methylation assays, such as strategy based on metal ion-mediated replication (Hong et al., 2017) and FRET-based MazF assays (Imanishi et al., 2017). The threshold time difference (ΔTt) was then plotted against the diverse ratios of methylated target m6A. According to Fig. 3D, the standard calibration curve exhibited good linearity between them. The linearly fitted line equation was $\Delta Tt = 71.16\ X + 3.45$ with a correlation coefficient of 0.991. Such a standard calibration curve can be used to directly assess the site-specific degree of methylation in a mixed RNA sample with a known total concentration. In order to further prove the accuracy of the TWJ-ECR assay, the synthetic m6A-RNA in different proportions was also detected by the EpiQuik m6A RNA methylation quantification kit. By comparing the two methods, we obtained consistent results (Fig. S4). The results proved a good consistency between the two methods.

We further investigated the sensitivity of the proposed platform by using different concentrations of target RNA. Various concentrations of target RNA were subjected to the TWJ-ECR assay and the produced fluorescence curves were measured in real-time manner. From Fig. S5A, with the concentration of m6A modification decreased, Tt value grew gradually. The ΔTt value was log-linear correlation with the concentration of target RNA. The correlation equation was $Y = 64.37 \log[C] + 716.80$ with a correlation coefficient of 0.983, where C denoted the concentration of target RNA (Fig. S5B).

3.4. Electrochemical detection of TWJ-ECR

In addition to fluorescent measurement, electrochemical detection has the advantages of miniaturization and portability (Zhou et al., 2021). Therefore, we extended the application of TWJ-ECR assay to the electrochemical platform. As shown in Fig. 1B, to realize the electrochemical transduction of the CRISPR detection signal, the fluorescent-labeled probe in the abovementioned strategy was substituted by methyl blue-labeled probe. Then the probes were immobilized on the electrode surface through the Au–S bond. The exponential amplification reaction time induced by the three-way junction was determined to be 80 min, according to the real-time fluorescence curve above (Fig. 3C). After the reaction, the products were incubated with CRISPR Cas12a to cleave the probes on the electrode (Fig. 1B). Besides, to increase the electrical conductivity of the glassy carbon electrode (GCE), Ce-MOF@Au was applied to as the electrode modification material. Meanwhile Ce-MOF@Au provided a large amount of connection sites for the probes (Fu et al., 2019).

3.4.1. Characterization of Ce-MOF and Ce-MOF@Au

The preparation of the Ce-MOF@Au was shown in Fig. 4A. Scanning electron microscopy (SEM) and transmission electron microscopy (TEM) in Fig. 4B suggested Ce-MOF had a good rod-like structure with a length ranging from 3 to 5 μm and a width from 100 to 200 nm, which was close to the literature report (Fu et al., 2019). The TEM and SEM images in Fig. 4C exhibited that the surface morphology of Ce- MOF@Au was rougher than that of Ce MOF, indicating many AuNPs within 20 nm in size were evenly distributed on the surface of Ce-MOF. Energy dispersive X-ray spectroscopy (EDS) spectrum in Fig. 4D suggested that the synthetic material contained Au and Ce. UV–visible spectroscopy (Fig. 4E) showed that Ce-MOF@Au not only had an obvious absorption peak near 210 nm of Ce-MOF, but also the characteristic peak of AuNPs at about 530 nm. In short, the morphology, element, and UV analysis all proved that Ce-MOF@Au was successfully synthesized.

3.4.2. Electrochemical characterization and feasibility of the fabricated biosensor

Fig. 5A described each step of the working electrode preparation. To verify whether the manufactured constructed electrochemical sensor can work as expected, cyclic voltammetry (CV) was conducted to characterize the changes on the surface of the electrochemical sensor after the stepwise modification. The CV curves of different modification steps on the electrode were displayed in Fig. 5B. The bare GCE exhibited a pair of clear redox peaks. When Ce-MOF@Au was modified on the bare GCE, a sharply increased peak current was observed. It is mainly attributed to large specific surface area and good electrical conductivity of Ce-MOF@Au. After the MB-modified reporter probes were immobilized on the GCE electrode, the redox peak current decreased owing to the electrostatic repulsion between the negatively charged probes and the negatively charged working buffer. With the addition of MCH to block non-specific sites, the redox peak current further decreased. That was attributed to the fact that the non-conductive material MCH hindered the efficiency of electron transfer. As a common electrochemical characterization method, electrochemical impedance spectroscopy (EIS)

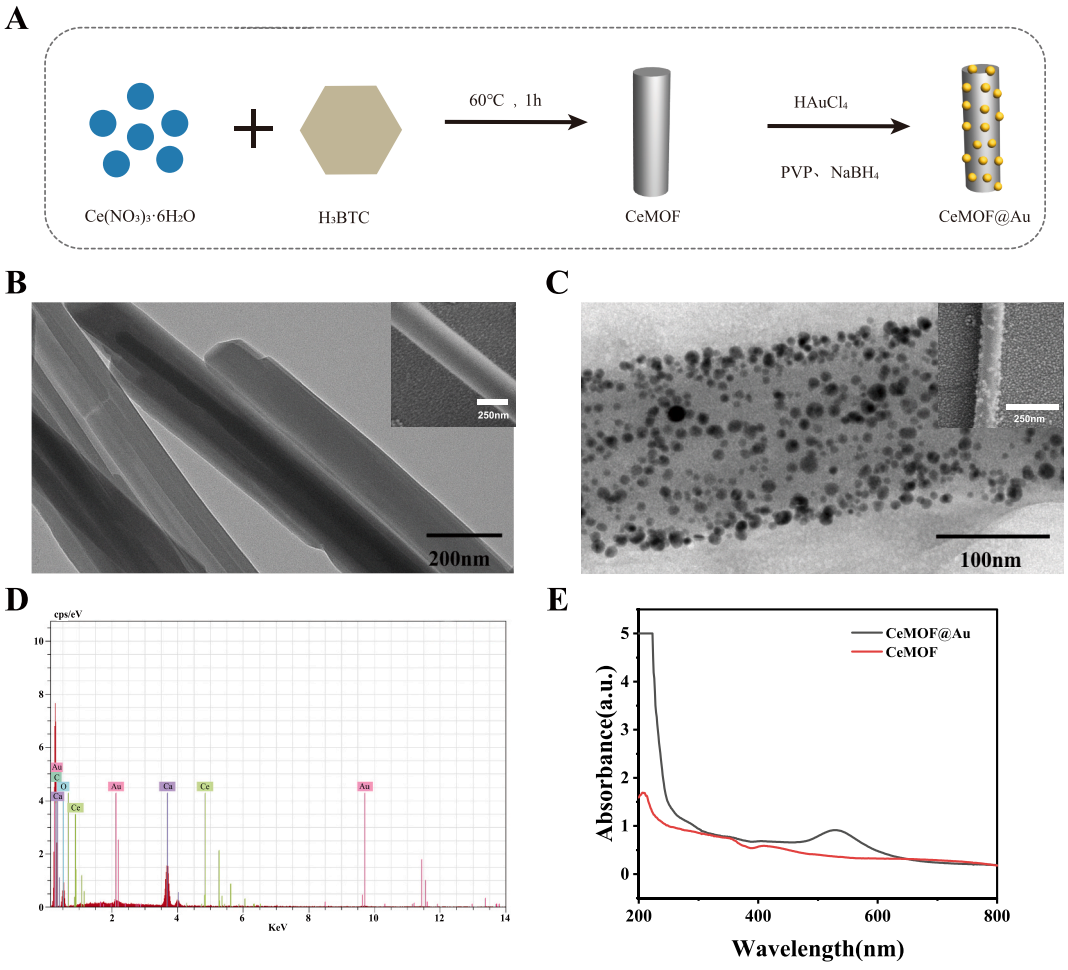


Fig. 4. Characterization of the materials. (A) The preparation of CeMOF@Au. (B) typical TEM image of CeMOF. Top right illustrated the SEM of CeMOF. (C) Typical TEM images of CeMOF@Au. Top right described the SEM of CeMOF@Au. (D) EDS pattern of CeMOF@Au. (E) UV–visible absorption of CeMOF and Ce-MOF@Au.

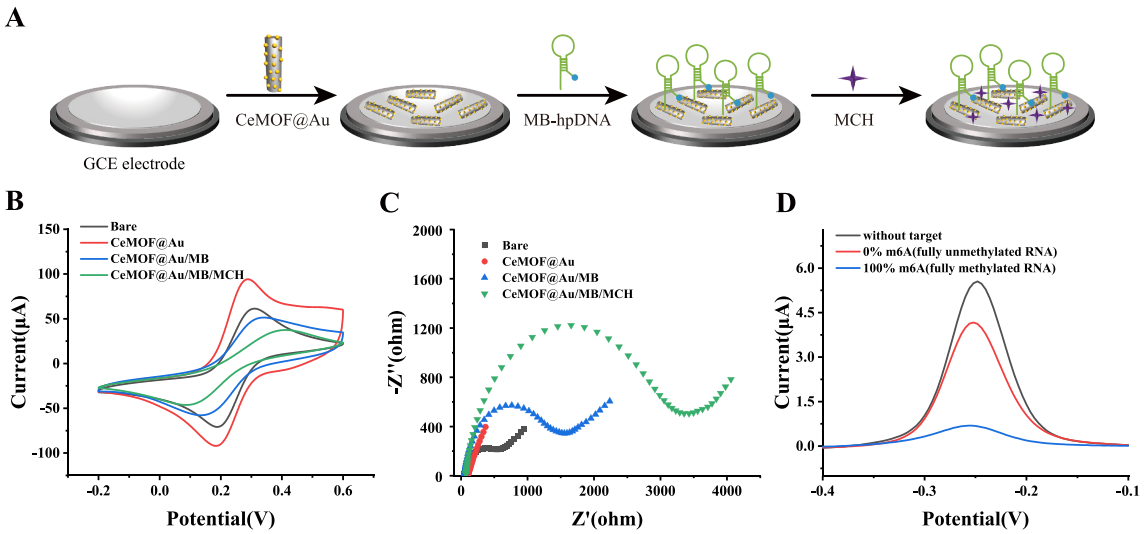


Fig. 5. Characterization of the electrode construction process. (A) Fabrication of working electrode stepwise assembly process. (B) CV and (C) EIS characterization of the electrodes at various steps of modification in a 5 mM $[Fe(CN)^6]^{3-/4-}$ solution. (D) SWV responses of different electrodes.

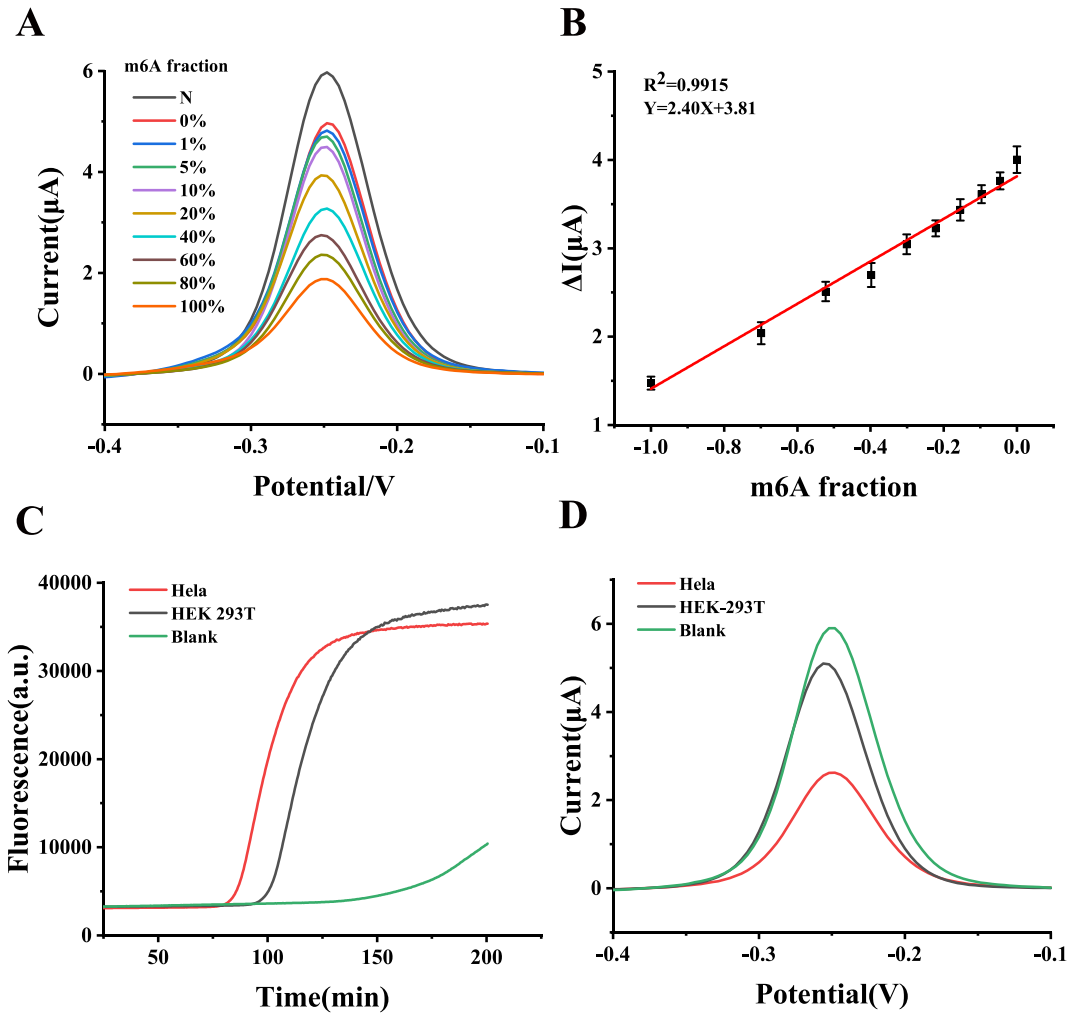


Fig. 6. Analytical performance of the electrochemical biosensor. (A) SWV responses of the sensor incubated with different ratios of m6A. (B) Linear relationship between the logarithm of various m6A fraction and ΔI values. ΔI represents the difference of SWV signal between target sample and blank sample. Real sample analysis. (C) Real-time fluorescence curves and (D) SWV current signals produced by the detection of MALAT1-2577 RNA extracted from HeLa cells and HEK293T cells. Error bars were obtained from triplicated independent experiments.

was also applied here for the stepwise characterization of modified electrodes. The results in Fig. 5C were consistent with the CV data, which further supports the successful construction of as-proposed sensor.

The SWV method characterized the electrochemical feasibility of the proposed m6A RNA detection method. We measured three sets of data including the blank, completely methylated RNA, and completely unmethylated RNA, and plotted the results in Fig. 5D. A high oxidation peak was observed at about - 0.25 V without target on account of the electroactive MB signal on the DNA hairpin stem. Compared with the blank control, when the products of completely unmethylated RNA were incubated with the Cas12a-crRNA complex, the electrode exhibited a slight decrease of the MB peak, indicating that completely unmethylated RNA hardly triggered this assay. Comparatively, the current became significantly weaker after adding the products produced from completely methylated RNA, which illustrated that Cas12a successfully cleaved the MB-modified reporter under the activation of the triggers. Hence, an electrochemical sensor for m6A detection was effectively constructed based on DNAzyme-triggered cleavage and signal amplification of TWJ-ECR.

3.4.3. Electrochemical analytical performance of the TWJ-ECR method for m6A RNA detection

To obtain the optical electrochemical sensing performance, probe density and cleavage time were optimized. The result of optimizing the probe density was described in Fig. S6. Accordingly, 1 μM probes and the cleavage time of 50 min were found to be the optimal conditions.

Under optimized experimental conditions, the proposed electrochemical biosensor was used to detect methylated m6A RNA with varying degrees of modification. Fig. 6A showed that the electrochemical response signals were generated by m6A modification in different proportions from 0% to 100%. A gradual decrease in current was observed as the degree of m6A modification continued to increase. As is shown in Fig. 6B, the change in current (ΔI value) was linearly dependent on the logarithm of the modification degree of m6A in the range of 10%–100%. A linear regression equation of $\Delta I = 2.40 \lg X + 3.81$ ($R^2 = 0.99$) was obtained, which was used to quantitatively detect the modification degree of target methylated RNA.

To verify the reproducibility of the sensor, ten electrodes were prepared in parallel under the same conditions and five replicate experiments were performed for fully methylated and fully unmethylated RNA, respectively. As profiled in Fig. S7A, the electrodes with the same methylation rate exhibited almost similar current response. All the results exhibited that the electrochemical sensor has superior reproducibility.

The stability of the sensor was assessed by detecting preserved fully methylated and fully unmethylated RNA for 3, 5, 7, and 10 days, respectively. The electrodes were infiltrated in 1 × PBS and stored in a refrigerator at 4 °C. The analytical results were depicted in Fig. S7B. Compared to the freshly prepared electrodes, 76.14% and 84.3% of the initial SWV signals were retained after 10 days, respectively, confirming that the constructed electrochemical sensors have good stability.

3.5. Real sample analysis

To verify the anti-interference ability of this method, two modified ratios of RNA (100% m6A and 0% m6A) in human serum were tested. As depicted in Fig. S8, compared with the TE buffer solution, either the Tt value in the constructed fluorescence sensor or the current signal in the electrochemical sensor had only a slight difference in serum. These results indicated that the present method has good anti-interference ability.

Fluorescence and electrochemical strategies were applied to detect site-specific methylation in total real RNA samples extracted from HEK293T cells and HeLa cells, respectively. Two types of cells (HeLa cells, HEK293T cells) were prepared for the assay, and it is known that the methylation levels in HeLa cells is slightly higher than that in HEK293T cells (Liu et al., 2013). As expected, Fig. 6C showed that the fluorescence response of the total RNA of HeLa cells was significantly faster than that of the total RNA of HEK293T cells. And the electrochemical results were consistent with the fluorescence data (Fig. 6D). These results all demonstrated that the proposed method could simply analyze the expression level of RNA methylation in cells.

The fat mass and obesity-associated enzyme (FTO) is an identified m6A demethylase, which removed methyl groups from m6A-containing substrates and convert m6A back to the original (Jia et al., 2011). To verify the demethylation ability of FTO, we treated total RNA extracted from HeLa cells and HEK293T with FTO. At the same time, the samples with demethylation inhibited with EDTA before FTO treatment were used as controls. The changes before and after the FTO treatment were detected through the fluorescence curve (Fig. S9). It can be seen that the Tt value increased after FTO treatment, proving that FTO did exert a demethylating effect.

4. Conclusion

In summary, we proposed a DNAzyme based TWJ-ECR strategy for antibody-free detection of site-specific m6A modifications for the first time. It utilized the merit of DNAzyme for specific cleavage of unmethylated RNA and the three-way junction to identify methylated RNA. After integration of EXPAR and CRISPR Cas12a assisted exponential amplification, it realized sensitive detection of m6A modifications down to 1% abundance. Besides, as-proposed sensing system demonstrated feasibility for the detection of complex biological samples and showed the potential for capability evaluation of demethylase. In addition, by designing different reporter DNA, this CRISPR/Cas12a-based sensing strategy was easily elaborated into multiple reactions for different detection purposes. And the fluorescence generated by CRISPR Cas was specifically triggered by the EXPAR products, which better reflected the reaction than using a nucleic acid dye such as SYBR Green. At last, because neither precise thermal cycling nor thermally stable enzyme was required, this isothermal amplification-based method is more applicable than RT-PCR. Overall, we expect that the constructed strategy would provide a new platform for the analysis of locus-specific m6A RNA in both biomedical studies and clinical precision medicine.

CRediT authorship contribution statement

Hongyan Yu: Methodology, Conceptualization, Investigation, Visualization, Validation, Data curation, Formal analysis, Writing – original draft. **Qinli Pu:** Investigation, Resources, Methodology, Formal analysis. **Zhi Weng:** Resources, Software, Formal analysis. **Xi Zhou:** Resources, Investigation. **Junjie Li:** Methodology, Conceptualization. **Yujun Yang:** Supervision, Methodology. **Wang Luo:** Resources, Methodology. **Huajian Chen:** Resources, Validation. **Guoming Xie:** Funding acquisition, Resources, Methodology, Supervision, Writing – review & editing, Project administration.

Declaration of competing interest

The authors declare that they have no competing interests.

Acknowledgments

This work was financially supported by the National Natural Science Foundation of China (81972025, 81802115) and the Graduate Scientific Research and Innovation Project of Chongqing (CYS20206).

Appendix A. Supplementary data

Supplementary data to this article can be found online at https://doi.org/10.1016/j.bios.2021.113625.

References

Alarcón, C.R., Goodarzi, H., Lee, H., Liu, X., Tavazoie, S., Tavazoie, S.F., 2015. Cell 162 (6), 1299–1308.

Boccaletto, P., Machnicka, M.A., Purta, E., Piatkowski, P., Baginski, B., Wirecki, T.K., de Crécy-Lagard, V., Ross, R., Limbach, P.A., Kotter, A., Helm, M., Bujnicki, J.M., 2018. Nucleic Acids Res. 46 (D1), D303–d307.

Chen, K., Lu, Z., Wang, X., Fu, Y., Luo, G.Z., Liu, N., Han, D., Dominissini, D., Dai, Q., Pan, T., He, C., 2015. Angew. Chem. Int. Ed. Engl. 54 (5), 1587–1590.

Choi, Y.C., Busch, H., 1978. Biochemistry 17 (13), 2551–2560.

Dai, Y., Somoza, R.A., Wang, L., Welter, J.F., Li, Y., Caplan, A.I., Liu, C.C., 2019. Angew. Chem. Int. Ed. Engl. 58 (48), 17399–17405.

Deng, X., Chen, K., Luo, G.Z., Weng, X., Ji, Q., Zhou, T., He, C., 2015. Nucleic Acids Res. 43 (13), 6557–6567.

Deng, X., Su, R., Weng, H., Huang, H., Li, Z., Chen, J., 2018. Cell Res. 28 (5), 507–517.

Ding, J.H., Ma, C.J., Chen, M.Y., Chen, B., Yuan, B.F., Feng, Y.Q., 2020. Anal. Chem. 92 (3), 2612–2619.

Dominissini, D., Moshitch-Moshkovitz, S., Schwartz, S., Salmon-Divon, M., Ungar, L., Osenberg, S., Cesarkas, K., Jacob-Hirsch, J., Amariglio, N., Kupiec, M., Sorek, R., Rechavi, G., 2012. Nature 485 (7397), 201–206.

Fu, L., Amato, N.J., Wang, P., McGowan, S.J., Niedernhofer, L.J., Wang, Y., 2015. Anal. Chem. 87 (15), 7653–7659.

Fu, X., He, J., Zhang, C., Chen, J., Wen, Y., Li, J., Mao, W., Zhong, H., Wu, J., Ji, X., Yu, C., 2019. Biosens. Bioelectron. 132, 302–309.

Harcourt, E.M., Ehrenschwender, T., Batista, P.J., Chang, H.Y., Kool, E.T., 2013. J. Am. Chem. Soc. 135 (51), 19079–19082.

Hong, T., Yuan, Y., Chen, Z., Xi, K., Wang, T., Xie, Y., He, Z., Su, H., Zhou, Y., Tan, Z.J., Weng, X., Zhou, X., 2018. J. Am. Chem. Soc. 140 (18), 5886–5889.

Hong, T., Yuan, Y., Wang, T., Ma, J., Yao, Q., Hua, X., Xia, Y., Zhou, X., 2017. Chem. Sci. 8 (1), 200–205.

Huang, W., Qi, C.B., Lv, S.W., Xie, M., Feng, Y.Q., Huang, W.H., Yuan, B.F., 2016. Anal. Chem. 88 (2), 1378–1384.

Imanishi, M., Tsuji, S., Suda, A., Futaki, S., 2017. Chem. Commun (Camb). 53 (96), 12930–12933.

Jia, G., Fu, Y., Zhao, X., Dai, Q., Zheng, G., Yang, Y., Yi, C., Lindahl, T., Pan, T., Yang, Y. G., He, C., 2011. ASC7 (12), 885–887.

Jia, H., Li, Z., Liu, C., Cheng, Y., 2010. Angew. Chem. Int. Ed. Engl. 49 (32), 5498–5501.

Jiang, Y.S., Bhadra, S., Li, B., Wu, Y.R., Milligan, J.N., Ellington, A.D., 2015. Anal. Chem. 87 (6), 3314–3320.

Kong, R.M., Zhang, X.B., Zhang, L.L., Huang, Y., Lu, D.Q., Tan, W., Shen, G.L., Yu, R.Q., 2011. Anal. Chem. 83 (1), 14–17.

Li, J., Yang, S., Zuo, C., Dai, L., Guo, Y., Xie, G., 2020. ACS Sens. 5 (4), 970–977.

Linder, B., Grozhik, A.V., Olarerin-George, A.O., Meydan, C., Mason, C.E., Jaffrey, S.R., 2015. Nat. Methods 12 (8), 767–772.

Liu, J., Harada, B.T., He, C., 2019. Trends Cell Biol. 29 (6), 487–499.

Liu, N., Parisien, M., Dai, Q., Zheng, G., He, C., Pan, T., 2013. RNA 19 (12), 1848–1856.

Makarova, K.S., Haft, D.H., Barrangou, R., Brouns, S.J., Charpentier, E., Horvath, P., Moineau, S., Mojica, F.J., Wolf, Y.I., Yakunin, A.F., van der Oost, J., Koonin, E.V., 2011. Nat. Rev. Microbiol. 9 (6), 467–477.

Marchand, V., Ayadi, L., Ernst, F.G.M., Hertler, J., Bourguignon-Igel, V., Galvanin, A., Kotter, A., Helm, M., Lafontaine, D.L.J., Motorin, Y., 2018. Angew. Chem. Int. Ed. Engl. 57 (51), 16785–16790.

Meyer, K.D., Saletore, Y., Zumbo, P., Elemento, O., Mason, C.E., Jaffrey, S.R., 2012. Cell 149 (7), 1635–1646.

Murakami, T., Sumaoka, J., Komiyama, M., 2012. Nucleic Acids Res. 40 (3), e22.

Peng, S., Tan, Z., Chen, S., Lei, C., Nie, Z., 2020. Chem. Sci. 11 (28), 7362–7368.

Sednev, M.V., Mykhailiuk, V., Choudhury, P., Halang, J., Sloan, K.E., Bohnsack, M.T., Höbartner, C., 2018. Angew. Chem. Int. Ed. Engl. 57 (46), 15117–15121.

Squires, J.E., Patel, H.R., Nousch, M., Sibbritt, T., Humphreys, D.T., Parker, B.J., Suter, C. M., Preiss, T., 2012. Nucleic Acids Res. 40 (11), 5023–5033.

Wang, P., Doxtader, K.A., Nam, Y., 2016a. Mol. Cell 63 (2), 306–317.

Wang, S., Wang, J., Zhang, X., Fu, B., Song, Y., Ma, P., Gu, K., Zhou, X., Zhang, X., Tian, T., Zhou, X., 2016b. Chem. Sci. 7 (2), 1440–1446.

Wei, C.M., Gershowitz, A., Moss, B., 1975. Cell 4 (4), 379–386.

Xing, S., Lu, Z., Huang, Q., Li, H., Wang, Y., Lai, Y., He, Y., Deng, M., Liu, W., 2020. Theranostics 10 (22), 10262–10273.

Yuan, C., Tian, T., Sun, J., Hu, M., Wang, X., Xiong, E., Cheng, M., Bao, Y., Lin, W., Jiang, J., Yang, C., Chen, Q., Zhang, H., Wang, H., Wang, X., Deng, X., Liao, X., Liu, Y., Wang, Z., Zhang, G., Zhou, X., 2020. Anal. Chem. 92 (5), 4029–4037.

Zetsche, B., Gootenberg, J.S., Abudayyeh, O.O., Slaymaker, I.M., Makarova, K.S., Essletzbichler, P., Volz, S.E., Joung, J., van der Oost, J., Regev, A., Koonin, E.V., Zhang, F., 2015. Cell 163 (3), 759–771.

Zhou, X., Pu, Q., Yu, H., Peng, Y., Li, J., Yang, Y., Chen, H., Weng, Y., Xie, G., 2021. J. Colloid Interface Sci. 599, 752–761.